Au enrichment and vertical relaxation of the Cu₃Au(111) surface studied by normal-incidence x-ray standing waves

O. Bauer,[1] C. H. Schmitz,[1] J. Ikonomov,[1] M. Willenbockel,[2] S. Soubatch,[2] F. S. Tautz,[2,3] and M. Sokolowski[1,*]

[1]*Institut für Physikalische und Theoretische Chemie der Universität Bonn, Wegelerstrasse 12, 53115 Bonn, Germany*

[2]*Peter Grünberg Institut (PGI-3), Forschungszentrum Jülich, 52425 Jülich, Germany*

[3]*Jülich Aachen Research Alliance (JARA), Fundamentals of Future Information Technology, 52425 Jülich, Germany*

We have investigated the $Cu_3Au(111)$ surface, prepared under ultrahigh vacuum conditions by sputtering and annealing, by low energy electron diffraction (LEED), scanning tunneling microscopy (STM), x-ray photoelectron spectroscopy, and normal incidence x-ray standing waves (NIXSW). We find the surface to be depleted with Cu and enriched with Au at the same time, yielding a nominal Cu:Au ratio of 0.61:0.39 in the topmost layer. The STM images reveal that the first layer is nearly closely filled with atoms and contains a small amount of vacancies with an area concentration of about 5%. Together with the Au enrichment, these cause local short-range disorder of the Au $p(2 \times 2)$ reconstruction. From this data, the average stoichiometry of the $p(2 \times 2)$ surface unit cell is estimated at $Cu_{2.22}Au_{1.44}\square_{0.20}$ (instead of $Cu_{3.00}Au_{1.00}\square_{0.00}$ of the ideal surface; $\square$ denotes an atomic vacancy site). From NIXSW we find a significant outward relaxation of both the Cu and Au atoms of the topmost layer by 0.28 Å and 0.33 Å, which corresponds to 13% and 15% of the (111) bulk layer spacing of Cu_3Au. We suggest that this originates from a widening of the first/second layer spacing, by 6.8% and 8.8% for the Cu and Au atoms, respectively, plus an additional rigid increase in the second/third layer spacing by 6.2%. We explain this by steric repulsions between Au atoms of the topmost layer, replacing smaller Cu atoms, and Au atoms in the second layer in combination with disorder. Finally, a lateral reconstruction, similar to that on the Au(111) surface, but with a much larger periodicity of 290 Å, is identified from LEED.

I. INTRODUCTION

The surface-near region, i.e., the selvedge, of a binary alloy can minimize its free energy both by stoichiometric and structural modifications with respect to the ideal bulk truncated surface. Hereby stoichiometric changes, resulting from surface segregation or depletion of one or the other element, are driven by the minimization of the surface tension, whereas structural modifications can be understood as a result of the related strain [1]. Evidently, the stoichiometric and structural parameters of binary alloys have to be determined and discussed for the specific surfaces and for the specific types of the interface, i.e., the bulk/vacuum or the bulk/electrolyte interface. In addition, in the case that kinetic limitations are relevant, the details of the route of preparation can matter.

In this manuscript, we report on the stoichiometry and the structure of the $Cu_3Au(111)$ surface, which has been less investigated so far compared with the (110) and (110) surfaces of Cu_3Au [1]. An ideal (111) surface terminated Cu_3Au crystal can be seen as a stack of (111) planes, each being composed of Cu and Au atoms in a ratio of 3:1, whereby the Au atoms are arranged in a $p(2 \times 2)$ submesh within the (111) planes. This arrangement is often referred to as the $p(2 \times 2)$ reconstruction with an ideal stoichiometry of Cu_3Au. So far, experimental results for the surface stoichiometry do not give a conclusive picture. Stierle *et al.* [2] reported an equal depletion of Cu and Au sites, both being occupied with only 70% probability. As a result the surface contains atomic vacancy sites. In this paper, we denote them by the symbol $\square$. Because of the depletion, the surface composition

reported by Stierle *et al.* [2] is $Cu_{0.525}Au_{0.175}\square_{0.300}$ instead of $Cu_{0.75}Au_{0.25}$ ($\square_{0.00}$) for the ideal surface. In addition, a surface inward relaxation of 2.3% was found [2]. Differently, Shaw and Fain reported Au enrichment, yielding a $Cu_{0.61}Au_{0.39}$ composition [3]. The Au enrichment is supported also by reflection electron microscopy experiments [4] and density functional theory (DFT) calculations [5]. The intention of the present paper is to clarify the situation on the clean surface using the high surface sensitivity of the normal incidence x-ray standing wave (NIXSW) method [6] for the determination of the vertical positions of the atoms in the surface layer in combination with photoemission for the determination of the surface composition of the vacuum prepared $Cu_3Au(111)$ surface. In addition, our paper was also motivated by follow-up experiments where we adsorbed organic molecules on this surface, which we will report in a second paper [7].

A. Experimental

We used two cut and polished $Cu_3Au(111)$ samples from the same commercially available rod. In order to restore and optimize the structural order after the polishing process in the surface near region, the samples were subject to a standard procedure after first insertion into the vacuum. It consisted of sputtering with argon for 30 min (800–1050 eV), annealing at 1000 K, i.e., above the order-disorder transition temperature T_0 at 663 K, for 15 min, cooling the sample slowly to 623 K (i.e., 40 K below T_0) at 1 Ks⁻¹, and finally annealing at 623 K for about 15 h in order to allow an optimal crystallization of the ordered Cu_3Au L1₂ phase [8]. Similar procedures have been used by other experimentalists and have proven to lead to good crystal order [9]. After this procedure the low energy electron diffraction (LEED) pattern showed a clear $p(2 \times 2)$

*Corresponding author: sokolowski@pc.uni-bonn.de

pattern of the Au reconstruction (see below). At later stages of the experiment, only shorter sputter cycles of 15 min followed by 60 min annealing at 623 K (i.e., below T_0) were used for removing surface contaminations.

In our home lab, the samples were subject to LEED measurements performed with a high resolution LEED system for spot profile analysis (SPA-LEED) [10] and scanning tunneling microcopy (STM) measurements on a RHK technology STM. Photoelectron spectroscopy and NIXSW experiments were made at the beamline ID 32 at the European Synchrotron Radiation Facility (ESRF) in Grenoble. Details concerning the electron analyzer used for these experiments are given in Ref. [11]. Important in the context of the present paper is that the setup is permitted to collect photoelectron at different emission angles, and hence with different surface sensitivities.

The NIXSW measurements were performed under near normal incidence geometry, at a Bragg angle $\Theta_B = 88°$, using the (111) reflection of the Cu_3Au substrate. The relevant $d_{(111)}$ lattice spacing of the Cu_3Au substrate is 2.165 Å [12,13], which corresponds to a Bragg energy E_B of 2865.04 eV at 300 K ($\Theta_B = 88°$). For obtaining the electron yield curves as a function of the photon energy [$Y(E)$], we recorded the photoemission (XP) and Auger spectra of the $Au3d_{5/2}$ level and the $CuL_3M_{45}M_{45}$ Auger transition at pass energies of 50 and 100 eV, respectively. For the determination of the surface composition, we measured the XP spectra of the $Cu2p_{3/2}$ and $Au3d_{5/2}$ levels and the $CuL_3M_{45}M_{45}$ Auger transition at 30 eV pass energy. There we used a photon energy of 2858.0 eV, i.e., 7 eV below the Bragg energy, in order to avoid standing wave field effects.

The acceptance angle of the electron analyzer was $\pm6°$ [14,15]. The axis of the electron analyzer was oriented at $90°$ with respect to the x-ray beam and horizontal, thus being identical with the polarization axis of the x-ray beam. Because the sample normal was tilted by $2°$ towards the analyzer, the analyzer axis corresponded to an electron emission angle θ of $88°$ with respect to the surface normal. Considering the limitation of the electron detection by the acceptance angle of the electron analyzer at $\theta_{min} = 88° - 6° = 82°$ and the self-shadowing effect of the sample crystal at $\theta_{max} = 90°$, this geometry corresponded to an *effective* electron emission angle, $\theta_{eff} = (\theta_{min} + \theta_{max})/2$, of $86°$ with respect to the sample normal. In this geometry, the escape depth of the photoelectrons is very small (see below). Hence atoms in the top-most surface layer contribute most dominantly to the photoelectron yield curves, and the NIXSW analysis yields the position of these. A second aspect of this detection geometry is also important for the data evaluation. The angle (θ_p) of the detected photoelectrons with respect to the polarization of the incident x-ray beam was limited to a small angular range close to $0°$ ($\theta_p = -2°$ to $6°$). For photoelectrons emitted exactly at $\theta_p = 0°$ and exactly parallel incident and reflected x-ray beams ($\Theta_B = 90°$), the nondipolar corrections for the photoemission process, which enter into the evaluation of the NIXSW yield curves, are expected to vanish [16,17]. Because the angular detection range was small and located close to $0°$ here and because the angle between incident and reflected x-ray beam was also small ($4°$), we made the reasonable assumption that for our detected electron yields the nondipolar corrections are very small and can be neglected. Thus, we analyzed the

photoelectron yield curves according to the NIXSW theory without nondipolar correction parameters.

In order to achieve some depth profiling of the elemental composition, we measured XP and Auger spectra for a series of different (effective) emission angles θ_{eff} of $86°$, $68°$, $48°$, and $28°$ by rotating the sample normal towards the analyzer. Upon decreasing emission angle θ_{eff}, the escape depth d_e of the photoelectrons increases, making the experiment more bulk sensitive. Using numerical values from Ref. [18], we calculated d_e for $\theta_{eff} = 86°$ to $28°$ to range from 1 to 10 Å for the $Au3d_{5/2}$ level and $CuL_3M_{45}M_{45}$ Auger transition and from 2 to 20 Å for the $Cu2p_{3/2}$ level, respectively. Comparing the numerical values of d_e with the layer spacing $d_{(111)}(Cu_3Au) = 2.165$ Å, we deduce that for $\theta_{eff} = 86°$ we dominantly probe the topmost surface layer. This surface-sensitive emission geometry ($\theta_{eff} = 86°$) was used for determining the elemental surface composition and for collecting NIXSW data. The NIXSW, XPS, and STM experiments were performed at room temperature; SPA-LEED data were recorded at 85 K.

II. RESULTS

A. Lateral order and surface composition

Figure 1(a) shows a LEED pattern of the surface, while Fig. 1(b) displays one-dimensional respective line scans at different energies. The six strong spots are fundamental spots of the averaged 1×1 mesh of Cu_3Au; the fainter spots (at smaller values of $|\mathbf{k}_{\parallel}|$) are related to the $p(2 \times 2)$ reconstruction of the Au atoms. No additional spots from pure islands of segregated Au or Cu can be detected. For the interpretation of the LEED data, one has to bear in mind that in addition to the topmost surface layer, lower layers also contribute with, however, attenuated intensity. The inverse full width at half maximum (FWHM) of the specular (0,0) spot is about 1000 Å at an electron energy (E) of 30 eV. This gives a lower estimate for the lateral diameter of the crystalline domains on the surface. With higher electron energies (E) the inverse FWHM decreases, i.e., to 400 Å at $E = 100$ eV, as it is typical for a metal crystal with some mosaic spread of the grains [19]. In agreement with STM results (see below), the surface is flat because we have no indications for high step densities from oscillations of the FWHM with energy. So far, these observations agree with our expectations on the basis of the bulk structure of Cu_3Au. We will now consider the more surface specific aspects.

Remarkably, the $p(2 \times 2)$ reconstruction spots are rather faint. The peak intensities of the first order spots of the $p(2 \times 2)$ reconstruction are, depending on the electron energy, by about a factor of 20 to 100 smaller than the specular (0,0) spot [see Fig. 1(b)]. Moreover, the inverse FWHM of these spots is found to be between 200 Å and 300 Å ($E = 30 - 100$ eV); hence the lateral coherence of the $p(2 \times 2)$ Au sublattices is smaller than that of the fundamental lattice (1000 Å) by about a factor of about 3 to 5. This indicates that lateral antiphase boundaries are present for the $p(2 \times 2)$ sublattice. Two reasons for the faintness of the $p(2 \times 2)$ spots can be envisaged. First, the spot intensities principally scale with the difference in the electron scattering factors of Cu and Au. Compared to the situation for x rays, the increase of the electron scattering
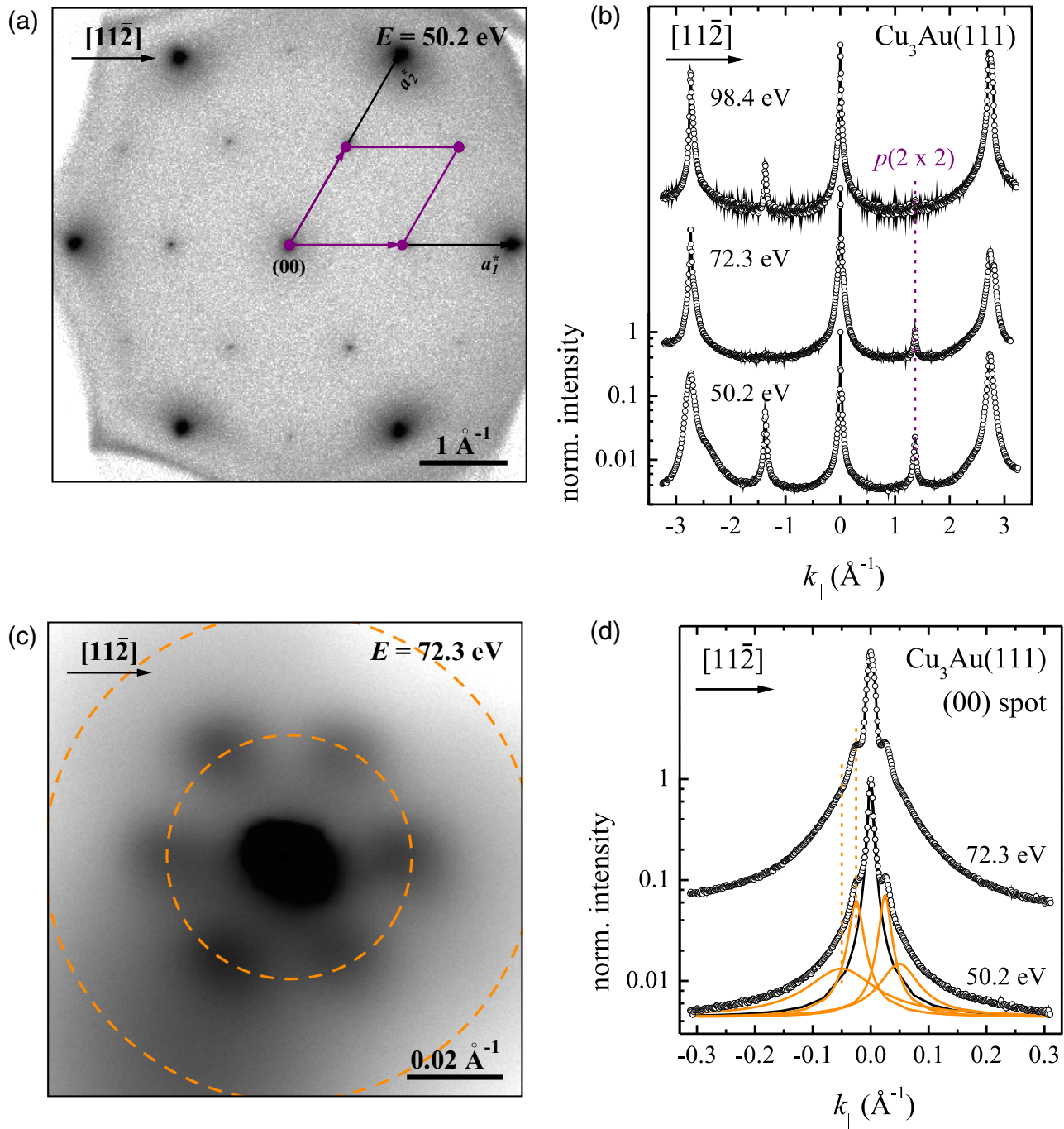
FIG. 1. One-dimensional LEED scans and two-dimensional LEED patterns of the clean $Cu_3Au(111)$ surface. The individual electron energies are specified in the respective figures. (a) Two-dimensional LEED pattern of the ordered $Cu_3Au(111)$ surface. The reciprocal lattice vectors $\mathbf{a}_i$ of the (disordered) substrate are indicated in black, while the unit cell of the $p(2 \times 2)$ reconstruction is indicated in purple. (b) One-dimensional LEED scans along the $[11\bar{2}]$ direction across the specular reflection at various electron energies. Note that the shoulder on the (10) substrate spot profile at $E = 72.3$ eV is an experimental artefact, absent at all other substrate spots. (c) Close up of the LEED pattern in (a) around the (0,0) spot. Dashed orange circles mark the radial positions of the first and second order long-range reconstruction spots. Note that the second-order spots can only be clearly discerned in one-dimensional LEED scans. (d) Close up of the one-dimensional LEED scans in (b) for two different energies. Lorentzian line shapes have been fitted to the spot profiles in (d). The orange colored profiles correspond to the first and second order spots of the long-range reconstruction. Note that the intense background around the first-order fundamental substrate spots in (a) and (b) for $E = 50.4$ eV was only observed at this particular electron energy and is absent for all other electron energies. All measurements were performed at 85 K except for the spot profile measurement at 98.4 eV in (b) ($T = 345$ K).
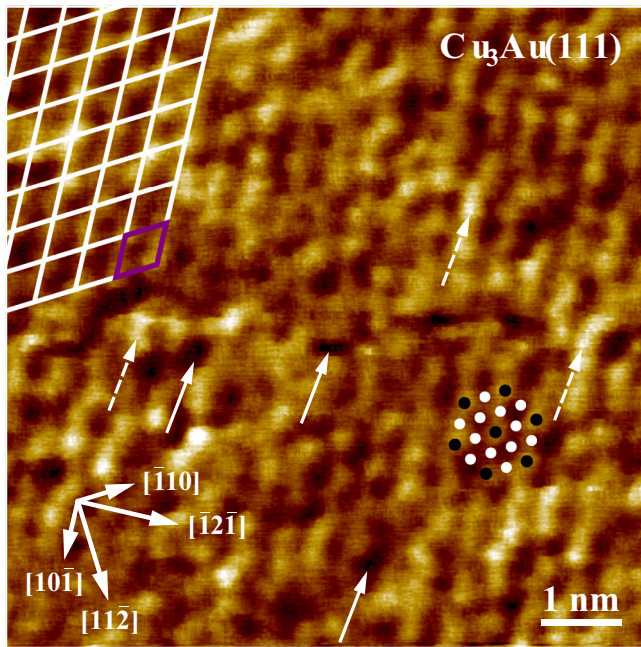
FIG. 2. The STM image of the clean $Cu_3Au(111)$ surface. Au atoms appear as bright protrusions. The ideal $Cu_3Au(111)$ surface is modeled by black (Au) and white circles (Cu). In addition, grid lines of the ideal $p(2 \times 2)$ reconstruction are superimposed in the upper left corner of the image, and the respective unit cell is marked in purple. The three white arrows mark exemplary dark defects, which we interpret by atomic vacancies in the topmost surface layer. The three dashed white arrows mark positions, which we interpret as Au atoms sitting on two next-neighbor lattice sites, thus partially substituting Cu atoms. The substrate directions are indicated. The STM image has been corrected for thermal drift (8 nm $\times$ 8 nm, $U_{bias} = -177$ mV, $I_t = -137$ pA). For further details see text.

factors with the atomic number is less systematic, and the scattering factors of Cu and Au can thus be more alike [20], which leads to small $p(2 \times 2)$ intensities. Second, as we will describe below, the $p(2 \times 2)$ structure of the surface layer is subject to short-range disorder. This also causes damping of the $p(2 \times 2)$ spots. However, a simple correlation of the $p(2 \times 2)$ spot intensity and the $p(2 \times 2)$ order in the surface layer is not possible because electrons diffracted by lower and better ordered layers, although attenuated, also contribute to the $p(2 \times 2)$ spots.

From detailed scans, we observe six satellites around the specular spot [see Figs. 1(c) and 1(d)]. These indicate the presence of a periodicity of long range of the surface. From careful fits to the line profiles [see Fig. 1(d)], we determined the distance of the satellites from the center of the specular spot. The corresponding periodicity is 290 ± 10 Å, and the corresponding wave vector is along the $[11\bar{2}]$ direction, i.e., perpendicular to the close-packed atomic rows. These satellites are reminiscent to those of the reconstruction of the pure Au(111) surface [21]. However, their azimuthal orientation is rotated by 30° with respect to those of the Au(111) surface. Before we interpret this reconstruction, we consider the STM and photoemission data.

Figure 2 shows an STM image with atomic resolution. Typically we find flat terraces with a lateral extension up to 1000 Å. The Au atoms are imaged as bright protrusions [22]. As indicated by the grid lines, the $p(2 \times 2)$ submesh of the Au atoms can be vaguely seen, although it is subject to lateral and non-lattice-matched displacements of the Au atoms from the ideal positions, inducing a significant disorder in the range of small correlation lengths, i.e., short-range disorder. In addition, some of the Cu positions of the ideal surface are occupied by Au atoms. This situation is encountered where two bright protrusions (assigned to Au atoms) are found at a next-neighbor distance in the STM image (exemplary marked by dashed white arrows in Fig. 2).

Finally, a small number of dark defects are visible in the STM image (marked by white arrows), which we interpret as atomic vacancies in the first layer. We estimate the area covered by these vacancies at about 5%. The short-range disorder of the $p(2 \times 2)$ that is seen in the STM images is in agreement with the LEED data, where we find sharp $p(2 \times 2)$ LEED spots but no spot broadening. Hence, the long-range order of the $p(2 \times 2)$ structure is maintained, although the structure undergoes local disorder. The preservation of the long-range order occurs by the interaction of the topmost surface layer with the underlying and more ordered (bulklike) second Cu_3Au layer. Therefore, the surface layer is in registry with the second layer and cannot be understood as a floating one. Figures 3(a) and 3(b) compare a hard sphere model of the ideal surface and the real surface, respectively. In the model of the real surface, we illustrate the structural disorder deduced from the STM data. In addition, the model accounts for the experimentally observed surface composition (see below).

From the integrated photoelectron and Auger electron yields, we calculated the respective ratios $\eta = Y(Cu2p_{3/2})/Y(Au3d_{5/2})$ and $\eta' = Y(CuL_3M_{45}M_{45})/Y(Au3d_{5/2})$. Within the scattering of the data, we find constant values of η and η' for different emission angles θ_{eff} of 68°, 48°, and 28° and consequently for different values of the escape depth d_e (see above) and corresponding effective thicknesses of the probed surface regions. Only for $\theta_{eff} = 86°$, i.e., for surface-sensitive emission geometry, we find values of η_s and η'_s (the index s denotes this special emission geometry), which are significantly smaller than the values found for η and η' otherwise [23]. This has to be interpreted as follows: The Cu:Au ratio is constant for all surface-near layers; only for the topmost surface layer it is reduced. Because we find constant values of η and η' independently of the escape depth d_e and no indication for a depth-related change of the composition, it is plausible and conclusive that all surface-near layers, except the topmost surface layer, exhibit the composition of the ideal Cu_3Au bulk, i.e., a Cu:Au ratio of 3:1.

Setting the elemental surface concentration ratio for the probed surface-near layers to three allows us to derive the elemental surface concentration ratios z and z' of the topmost surface layer, $z = 3\eta_s/\eta$ and $z' = 3\eta'_s/\eta'$ from ratios of the photo and Auger electron yields, respectively. We note that this procedure circumvents the uncertainties related to the photoelectron emission cross sections. We obtain $z = 1.53 \pm 0.06$ and $z' = 2.42 \pm 0.14$. Both values indicate the same trend of a decreased Cu:Au ratio at the surface versus the bulk ratio of three. However, we suppose that the z value is more
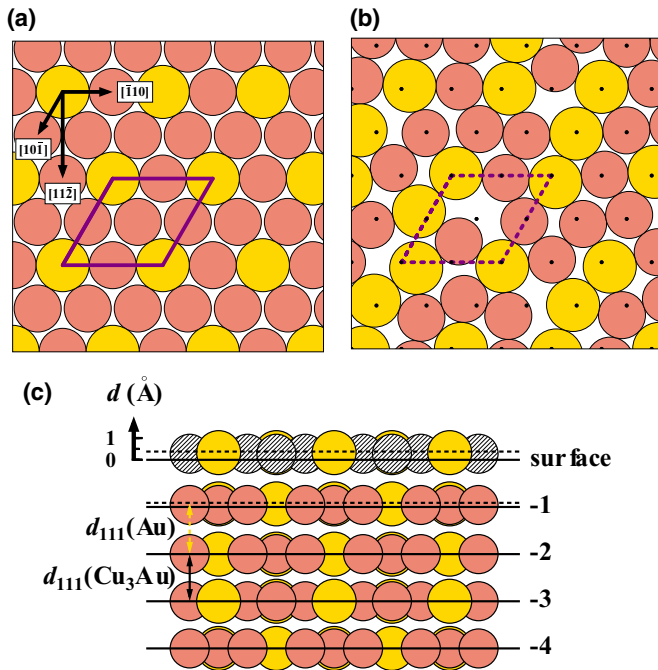
(a) **(b)**

(c)

FIG. 3. Schematic hard sphere models of (a) the ideal and (b) the real $Cu_3Au(111)$ surface. Cu and Au atoms are depicted in respective colors. The unit cell of the $p(2 \times 2)$ reconstruction is shown in purple. Black dots in (b) mark the atom positions expected for the ideal $Cu_3Au(111)$ surface [depicted in (a)]. The substrate directions are indicated. Note that the atoms are depicted at 97.5% of their metallic radii in order to avoid overlap of the spheres. (c) Schematic representation of the outward relaxation of the clean $Cu_3Au(111)$ surface. The $Cu_3Au(111)$ substrate is shown in a side view along the $[11\bar{2}]$ direction. The cut through the crystal is made along the $[\bar{1}10]$ direction at the position of a densely packed row of alternating Cu and Au atoms; (a) shows the crystallographic directions. The (111) lattice planes of the ideal Cu_3Au crystal are indicated by solid lines with separation of $d_{(111)}(Cu_3Au) = 2.165$ Å. These correspond to the extended (111) planes. The two dashed lines indicate hypothetic layer positions of the surface and -1 layer for assumed separations between the surface/-1 layer and the $-1/-2$ layer of $d_{111}(Au) = 2.355$ Å. The experimentally derived layer positions are close, but not identical, to the dashed lines (see text). Both the surface and the -1 layer are drawn with a small buckling of 0.05 Å between the Au and Cu atoms. For simplicity, further buckling within the Cu or Au atoms is not included. Cu atoms in the surface layer are drawn as hashed circles in order to indicate depletion. Note that the atoms are depicted at 70% of their metallic radii for reasons of clarity.

reliable than z' for experimental reasons: The background of the $CuL_3M_{45}M_{45}$ Auger signal is much broader, varies with θ_{eff}, and is thus more difficult to subtract from the signal, leading to a too large value of z'.

From $z = 1.53 \pm 0.06$, we calculate a surface composition of $Cu_{0.605}Au_{0.395}$ (instead of $Cu_{0.75}Au_{0.25}$ of the ideal surface). The Au surface concentration is $x_{Au} = 0.395 \pm 0.01$ instead of 0.25 for the ideal surface. Hence, the topmost surface layer is considerably enriched with Au and depleted with Cu in agreement with the STM data. Assuming that the sum of the geometric cross sections of the surface atoms ($\sum_i \pi r_i^2$) is the same for the ideal and the real surface [r_i being the metallic

radii, $r_i(Cu) = 1.28$ Å, $r_i(Au) = 1.44$ Å [24]], we calculate that the $p(2 \times 2)$ unit cell has an average stoichiometry of $Cu_{2.34}Au_{1.52}$ instead of $Cu_{3.00}Au_{1.00}$ of the ideal surface. This means that 0.66 of the smaller Cu atoms per $p(2 \times 2)$ unit cell have been replaced by 0.52 of the larger Au atoms. As a consequence, the surface layer is enriched with Au and contains a smaller number of atoms compared to the ideal $Cu_3Au(111)$ surface.

However, the size difference of atoms in metallic alloys is usually reduced, and, moreover, some precaution should also be taken when transferring these bulk-derived radii to a surface. Hence, an alternative estimation for the limit of equal radii for Cu and Au is instructive. There we calculate $Cu_{2.42}Au_{1.58}$, meaning that 0.58 Cu atoms per $p(2 \times 2)$ unit cell are replaced by the same number of Au atoms. So far, these calculations do not take into account the approximately 5% surface vacancies (which we denote by $\square$) seen by STM. If this is done, we obtain average stoichiometries of the $p(2 \times 2)$ unit cell, for the cases of different and equal atomic radii, of $Cu_{2.22}Au_{1.44}\square_{0.20}$ and $Cu_{2.30}Au_{1.50}\square_{0.20}$, respectively.

We now come back to the long-range surface reconstruction that is seen in LEED from the presence of small satellite spots around the (0,0) spot. The first model would be that the lattice constant of the top-most layer is slightly (linearly by $\sim 1\%$) expanded. This would make the top layer incommensurate to the second and deeper layers. Due to multiple electron scattering or *Moire* effects [25], one would indeed expect the appearance of additional spots at the positions of the observed satellites. Two facts stand against this. First, from STM images revealing the existence of a $p(2 \times 2)$ superstructure at the surface in combination with sharp superstructure spots seen in LEED, we know that the top layer is in registry with the second layer and, hence, cannot be incommensurate. Second, for an incommensurate top layer much stronger intensities of the satellites would be expected due to the strong contribution of the top layer to the scattered intensities. Such a situation is encountered, e.g., on the reconstructed Au(111) surface [26], where the top layer is compressed with respect to the second layer. Hence we favor a second model where the registry of the top layer to the underlying layers is only locally lost, namely on a periodic network of domain walls, which separate domain cores in which the registry and the commensurability of the top layer to the second layer is maintained. The periodic arrangement of the domain walls causes the appearance of the satellite spots. We suppose that within the domain walls the area density of the atoms is locally higher compared to the domain cores, and the registry to the second layer is locally lost. The atoms in the domain walls possibly undergo vertical out-of-the-surface displacements which reduce the stress. The distance between the domain walls is indeed very large (~ 100 lattice constants in diameter). We note that large distances between line defects (~ 40 lattice constants) were observed, e.g., on the Pt(111) surface [27], and similar satellites were detected there with surface sensitive x-ray diffraction [28]. We have not been able to identify the domain walls in our STM data; possibly they are hidden by the strong chemical contrast between Au and Cu atoms. Obviously, the above two models resemble two extreme points and can be gradually transformed into each other. From the data so far, we favor the second model.

Summarizing at this stage, the topmost layer of the Cu_3Au surface is enriched with Au. The Au atoms statistically replace Cu atoms at the surface. Due to the larger size of the Au with respect to the Cu atoms, this leads to displacements of surface atoms from ideal lattice positions and causes a short-range disorder of the $p(2 \times 2)$ reconstruction, as illustrated in Fig. 3(b). Nevertheless, the long-range order is maintained via the registry of the top layer to the second layer.

B. Surface relaxation

Figure 4(a) displays the x-ray reflectivity (Darwin-Prins) curve [$R(E)$], and Fig. 4(b) shows the normalized photoemission yield curves Y_{Zj} of the $Au3d_{5/2}$ and $CuL_3M_{45}M_{45}$ signals. Using the structure factors of the ideal Cu_3Au bulk, a good fit of $R(E)$ is obtained. The fit reproduces the Bragg energy expected on the basis of the bulk (111) layer spacing (2.165 Å). This indicates that the Cu_3Au bulk is mainly as expected. Nevertheless, we see small systematic deviations of the theoretically calculated $R(E)$ curve from the experimental, e.g., at the top of the curve and in the asymmetry at the flanks, that are slightly larger than those usually encountered for metal crystals. We speculate that these may be related to a
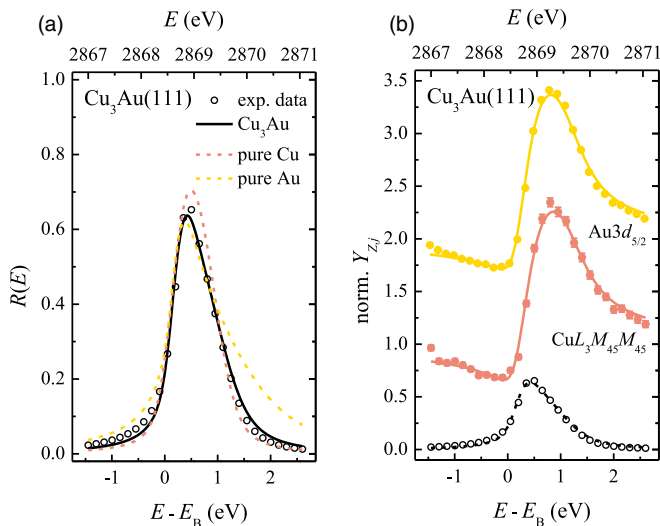

FIG. 4. (a) Typical Darwin-Prins curve $R(E)$ of the (clean) $Cu_3Au(111)$ substrate crystal (black open circles; error bars have been omitted for clarity). The reflectivity of the substrate was measured employing the (111) lattice planes. The corresponding fit is shown as a black solid line. In addition, two fitting curves are shown as dashed lines in respective colors where the substrate was modeled as being composed of either Cu or Au atoms only. (b) Typical XSW photoelectron yield curves of Cu and Au at the clean $Cu_3Au(111)$ surface. The $CuL_3M_{45}M_{45}$ and $Au3d_{5/2}$ signals were employed in the respective XSW experiments. Experimental data points are shown as filled circles, while respective fits to the data are shown as solid lines. The curves have been vertically offset for clarity. Error bars are so small that they are almost hidden by the data points. In addition, the measured reflectivity of the substrate employing the (111) lattice planes (open circles) and the corresponding fit (dashed line) are shown [same data as in (a)]. Error bars have also been omitted for clarity here. Note that only the topmost surface layer has been probed in these experiments.

TABLE I. Averaged values of the coherent fractions (f_c) and coherent positions (p_c) of the Cu and Au atoms, obtained from averaging the results of three data sets each. The d_c values are calculated as $p_c \times d_{(111)}$ (Cu_3Au), where $d_{(111)}(Cu_3Au) = 2.165$ Å is the lattice plane spacing corresponding to the (111) Bragg reflection that was probed here.

	f_c	p_c	d_c (Å)
Cu	0.82(5)	0.13(1)	0.28(1)
Au	0.81(7)	0.15(1)	0.33(2)

small deviation from the 3:1 stoichiometry in the bulk due to additional Cu atoms or Au vacancies and/or disorder of the Au superstructure. However, so far we have refrained from fixing these small deviations by using more elaborate models for the Cu_3Au bulk. Nevertheless, we have systematically confirmed that the impact of such a refinement on fitted values of the coherent positions (p_c) and fractions (f_c) would be within the statistical errors, which proves our results to be meaningful. Recently, we have been informed that, alternatively, the noted deviations could also be due to a small unwanted contribution of x-ray intensity from a higher order reflection of the x-ray beam monochromator [29].

For an illustration of the impact of a variation of the stoichiometry, $R(E)$ curves based on the structure factors of pure Cu or Au, but calculated for the observed Cu_3Au bulk layer spacing, are also displayed in Fig. 4(a). The $R(E)$ curve calculated for Au deviates from the experimental on both flanks of the peak, in particular on the high energy side, while the $R(E)$ curve calculated for Cu fits much better, as it is expected from the 3:1 stoichiometry of Cu:Au. The fit of the yield curves of Cu and Au [Fig. 4(b)] can be considered as very good; shortcomings in the fit of the $R(E)$ curve have only a marginal effect here. Already the visual inspection of the yield curves reveals the Au and Cu surface atoms being at very similar heights. The fitted p_c and f_c values are given in Table I, together with the absolute heights d_c of the surface atoms with respect to the position of the ideal surface given by the extended (111) lattice planes of the Cu_3Au bulk. The Cu and Au atoms are found to be 0.28 and 0.33 Å above the ideal surface, respectively. Hence, a substantial relaxation of these atoms into the vacuum by 13% (Cu) and 15% (Au) of $d_{(111)}(Cu_3Au) = 2.165$ Å occurs. In addition, we find f_c values (for Cu and Au), which are about 20% smaller than 1, the value that is expected for an ideal flat surface, and still 10% smaller than the values typically found for clean metal crystals, e.g., for Ag(100), $f_c = 0.90$ is obtained with the same experimental setup [30]. This indicates some buckling of the surface, likely due to the disorder that is present. An oversimplified two level model with two distinct and equally occupied levels would reproduce these f_c values for vertical displacements of ± 0.16 to ± 0.22 Å. This range of values appears reasonable when compared to the buckling of the reconstructed Au(111) surface, for which values of the vertical displacements between ± 0.15 to ± 0.20 Å have been reported [21,31,32]. Notably, our f_c values agree within the error with those reported by Tolkiehn *et al.* for the (200) Bragg reflection measured on a $Cu_3Au(100)$ surface ($f_c = 0.82/0.83 \pm 0.02$) [33].

How do we have to interpret this strong outward relaxation of the topmost surface atoms? Obviously, the relaxation is due to an increase of the separation between the layers near to the surface. The model we discuss in the following is illustrated in Fig. 3(c). From our data, we cannot firmly derive how the different surface-near layers contribute to the total relaxation of the topmost layer that we measure. However, it is reasonable to assume that the spacing between Au atoms in the topmost and the first subsurface layer [labeled with -1 in Fig. 3(c)] is not larger than that between the (111) layers of a pure Au crystal, i.e., 2.355 Å. This corresponds to an increase with respect to the (111) layer distance of the ideal Cu_3Au bulk (2.165 Å) by 8.8%. Considering the Au surface atoms, it implies that the rest of the observed total relaxation given by $p_c = 15\%$, namely $15\% - 8.8\% = 6.2\%$, has to be attributed to an expansion of the spacing $d_{-1/-2}$ between the -1 and -2 layer. This yields $d_{-1/-2} = 2.300$ Å. Of course, these arguments apply only to the Au atoms in first instance. However, the p_c of the Cu atoms is only by 0.02 smaller compared to the p_c of the Au atoms. The Cu atoms are hence by 0.05 Å lower in the top surface layer than the Au atoms, causing some small Au/Cu buckling. However, the respective height difference is much smaller than the relaxation itself, and the Cu_3Au surface layer apparently relaxes essentially as a rigid layer. A rigid layer behavior is hence plausible for the -1 layer, too. Conclusively, we feel safe to expand our above given arguments given for Au atoms to the Cu atoms of the -1 layer, which means that the Cu atoms follow the relaxation of the Au atoms in the -1 layer and relax also by 6.2% with respect to the -2 layer. Of course, we cannot exclude small height differences of the same order as in the surface layer between the Cu and Au atoms in the -1 layer, i.e., that the -1 layer shows some residual Au/Cu buckling. However, this would have only a very minor influence on the structure, as illustrated in Fig. 3(c). The described model attributes 60% of the relaxation to the topmost layer spacing and 40% to the second layer spacing. Figure 3(c) illustrates this situation. Of course different models, e.g., with contributions of 60%, 30%, and 10% of the topmost three layers to the relaxation, are also compatible with our data.

Two small final amendments are to be made. By surface x-ray scattering, a relaxation of the reconstructed Au(111) surface by +3% was derived [34], yielding $d_{0/-1} = 2.426$ Å. To use this value as the upper reasonable limit for $d_{0/-1}$ of the Cu_3Au(111) surface is also plausible. It yields a correspondingly smaller expansion of $d_{-1/-2}$ by only 2.9% instead of 6.2% calculated above. The second amendment concerns the contribution of deeper layers to the photoelectron signal. So far, we made the well-reasoned assumption that the photoelectron signals stem exclusively from the topmost surface layer and that the retrieved coherent positions (p_c) correspond to the displacement of atoms in the surface layer. One may hence ask whether possible contributions of deeper layers could misleadingly lead to a too large surface relaxation. Fortunately, this cannot be the case because due to smaller displacements of the deeper layers their contributions would reduce the weighted average of p_c. This misleading situation would be only encountered if the vertical displacements of the deeper layer from the extended (111) planes surpassed the displacement of the surface layer considerably. This, however, is unreasonable.

III. DISCUSSION

Our observed Au enrichment ($x_{Au} = 0.395 \pm 0.010$) of the Cu_3Au(111) surface after preparation in ultrahigh vacuum (UHV) is in good agreement with the findings of other experimentalists. Shaw and Fain found $x_{Au} = 0.39$ [3]; Moreira *et al.* derived a strong Au segregation from lab-based XPS data [5]. Theoretical approaches also point in this direction, predicting x_{Au} between 0.50 and 0.75 [5] or $x_{Au} = 0.40$ [35]. Notably, the Au segregation was found to be limited to the topmost layer [5,35], which agrees with the conclusions from our data. Concerning the outward relaxation, the agreement with predictions based on DFT is not as good. Moreira *et al.* found outward relaxations of the 2 Au atoms per surface unit cell (Cu_2Au_2) of 0.10 and 0.21 Å. These values are both smaller than the value of 0.33 Å we observed. In addition, Moreira *et al.* found only marginal relaxations of the Cu atoms. This is in contradiction to our observation. We find that the surface relaxes as whole, like a *rigid* planar layer, because the height difference $d_c(\text{Au}) - d_c(\text{Cu})$ amounts to 0.05 Å only. We suppose that this discrepancy may be due to the smallness of the unit cell used by Moreira *et al.* for their DFT calculations [5].

Interestingly, as described above, we have to conclude that the topmost *and* at least the second layer relax outward. We explain the increase in the first layer spacing by repulsive interactions between Au atoms in the top layer and in the second layer at Au-to-Au contact points. Such contacts are absent in the ideally ordered Cu_3Au bulk, but they are created immediately when Cu atoms in the topmost layer are replaced by Au atoms. Due to the larger metallic radius of Au compared to Cu, the Au-to-Au contact points impose locally larger spacings to the second layer that apparently cause a rigid shift of the entire top layer into the vacuum. In addition, the local disorder in the $p(2 \times 2)$ reconstruction has the same effect. It also causes the fact that Au atoms in the topmost layer are shifted away from their original threefold hollow sites, given by three Cu atoms of the second layer, leading to Au-to-Au contact points between the topmost and second layer again. The widening of the first layer spacing is thus a direct consequence of Au atoms at the original positions of Cu atoms due to the Au enrichment and disorder. In addition to this effect, electronic effects from the replacement of Cu by Au may play a role.

For explaining the increase in the distance between the second and third layer, we suppose that some lateral disorder in the $p(2 \times 2)$ reconstruction is also present in the second layer, although it is possibly smaller than that in the topmost layer. As a consequence, repulsive Au-to-Au contacts between the second and third layer are established likewise as between the topmost and second layer, which cause a widening of this layer distance, too. This mechanism is effective, even if the second layer already exhibits the intrinsic bulk stoichiometry, as indicated by our XPS data. In the case of a small Au enrichment (compatible with the systematic errors of our XPS data) in the second layer, this effect would contribute additionally.

Where do the Cu atoms of the topmost layer go when being replaced by Au atoms? Because we did not observe enrichment of Cu in the second or deeper layers, we assume the Cu atoms to diffuse deeply into the bulk. Alternatively, they could

have desorbed from the sample during the annealing cycle at 1000 K, which appears to be compatible with the estimated vapor pressure of Cu [36]. In addition, some of the Cu atoms could play a role for the line defects we have discussed as the origin of the lateral surface reconstruction of long range (290 Å). This surface reconstruction itself can be understood as a consequence of the compressive strain that is applied to the surface due to the substitution of Cu by the larger Au atoms. This strain possibly induces an outward displacement of the Au atoms at specific positions, locally similar to the situation on the reconstructed Au(111) surface, although the periodicity of the reconstruction is by about a factor of four larger.

IV. SUMMARY

We found the UHV-prepared $Cu_3Au(111)$ surface to be significantly enriched with Au in the surface layer, leading to an average stoichiometry of the $p(2 \times 2)$ unit cell of $Cu_{2.22}Au_{1.44}$ (instead of $Cu_{3.00}Au_{1.00}$ of the ideal surface). This enrichment causes short-range disorder of the $p(2 \times 2)$ reconstruction and has a strong effect on the layer separations between the topmost and second as well as the second and third layers. These move towards the vacuum by 8.8% and 6.2% with respect to their position in the ideal crystal.

[1] M. A. Vasiliev, J. Phys. D **30**, 3037 (1997).

[2] A. Stierle, A. Steinhauser, A. Ruhm, F. U. Renner, R. Weigel, N. Kasper, and H. Dosch, Rev. Sci. Instrum. **75**, 5302 (2004).

[3] G. C. Shaw and S. C. J. Fain, in *Proceedings of the Seventh International Vacuum Congress and the Third International Conference on Solid Surfaces of the International Union for Vacuum Science, Technique and Applications*, edited by R. Dobrozemsky, F. Rüdenauer, F. P. Viekböck and A. Breth (F. Berger & Söhne, Horn, Austria, 1977), Vol. III, pp. 2315–2318.

[4] Y. Huang, M. Gajdardziska-Josifovska, and J. M. Cowley, Ultramicroscopy **57**, 391 (1995).

[5] M. D. Moreira, G. N. Fontes, H. Niehus, C. A. Achete, and R. B. Capaz, J. Vac. Sci. Technol. B **30**, 051802 (2012).

[6] D. P. Woodruff, Rep. Prog. Phys. **68**, 743 (2005).

[7] O. Bauer, J. Ikonomov, C. H. Schmitz, M. Willenbockel, S. Soubatch, F. S. Tautz, and M. Sokolowski, Phys. Rev. B (unpublished).

[8] H. Okamoto, D. J. Chakrabarti, D. E. Laughlin, and T. B. Massalski, J. Phase Equilib. **8**, 454 (1987).

[9] H. C. Potter and J. M. Blakely, J. Vac. Sci. Technol. **12**, 635 (1975).

[10] M. Horn-von Hoegen, Zeitschrift für Kristallographie - Crystalline Materials **214**, 684 (1999).

[11] G. Mercurio, O. Bauer, M. Willenbockel, N. Fairley, W. Reckien, C. H. Schmitz, B. Fiedler, S. Soubatch, T. Bredow, M. Sokolowski, and F. S. Tautz, Phys. Rev. B **87**, 045421 (2013).

[12] R. W. G. Wykoff, *The Structure of Crystals* (Chemical Catalog Company, New York, USA, 1931).

[13] H. Dosch, L. Mailänder, H. Reichert, J. Peisl, and R. L. Johnson, Phys. Rev. B **43**, 13172 (1991).

[14] J. Duvernay, ESRF, private communication, April 2011.

[15] Specs Surface Nano Analysis GMBH, PHOIBOS HV Series: PHOIBOS 150 HV and PHOIBOS 225 HV Analyzers for Hard X-ray Photoelectron Spectroscopy (product brochure), Berlin, Germany (2013).

[16] D. P. Woodruff, Nucl. Instrum. Methods Phys. Res., Sect. A **547**, 187 (2005).

[17] I. Vartanyants, T.-L. Lee, S. Thiess, and J. Zegenhagen, Nucl. Instrum. Methods Phys. Res., Sect. A **547**, 196 (2005).

[18] S. Tanuma, C. J. Powell, and D. R. Penn, Surf. Interface Anal. **17**, 911 (1991).

[19] M. Sokolowski and H. Pfnür, Phys. Rev. B **49**, 7716 (1994).

[20] M. A. V. Hove, W. H. Weinberg, and C.-M. Chan, *Low-Energy Electron Diffraction, Experiment, Theory and Surface Structure Determination* (Springer, Berlin1986).

[21] J. V. Barth, H. Brune, G. Ertl, and R. J. Behm, Phys. Rev. B **42**, 9307 (1990).

[22] L. G. Dias, A. A. Leitão, C. A. Achete, R. P. Blum, H. Niehus, and R. B. Capaz, Surf. Sci. **601**, 5540 (2007).

[23] Oliver Bauer, Surface bonding of a functionalized aromatic molecule: Adsorption configurations of PTCDA on coinage metal surfaces, Ph.D. thesis, University of Bonn, 2015 (urn:nbn:de:hbz:5n-42331), available at http://hss.ulb.uni-bonn.de/2015/4233/4233.htm.

[24] M. Trömel and S. Hübner, Zeitschrift für Kristallographie - Crystalline Materials **215**, 429 (2000).

[25] M. Meissner, M. Gruenewald, F. Sojka, C. Udhardt, R. Forker, and T. Fritz, Surf. Sci. **606**, 1709 (2012).

[26] L. Kilian, E. Umbach, and M. Sokolowski, Surf. Sci. **600**, 2633 (2006).

[27] M. Hohage, T. Michely, and G. Comsa, Surf. Sci. **337**, 249 (1995).

[28] G. Grübel, K. G. Huang, D. Gibbs, D. M. Zehner, A. R. Sandy, and S. G. J. Mochrie, Phys. Rev. B **48**, 18119 (1993).

[29] C. Kumpf (private communication, 2015).

[30] O. Bauer, G. Mercurio, M. Willenbockel, W. Reckien, C. Heinrich Schmitz, B. Fiedler, S. Soubatch, T. Bredow, F. S. Tautz, and M. Sokolowski, Phys. Rev. B **86**, 235431 (2012).

[31] C. Wöll, S. Chiang, R. J. Wilson, and P. H. Lippel, Phys. Rev. B **39**, 7988 (1989).

[32] M. Corso, L. Fernández, F. Schiller, and J. E. Ortega, ACS Nano **4**, 1603 (2010).

[33] M. Tolkiehn, D. V. Novikov, and S. S. Fanchenko, Phys. Rev. B **71**, 165404 (2005).

[34] A. R. Sandy, S. G. J. Mochrie, D. M. Zehner, K. G. Huang, and D. Gibbs, Phys. Rev. B **43**, 4667 (1991).

[35] M. Hou and M. ElAzzaoui, Surf. Sci. **380**, 210 (1997).

[36] H. N. Hersh, J. Am. Chem. Soc. **75**, 1529 (1953).